Materials Science and Engineering A 391 (2005) 104–113

MATERIALS SCIENCE & ENGINEERING A

www.elsevier.com/locate/msea

In situ observations of lattice expansion and transformation rates of α and β phases in Ti–6Al–4V

J.W. Elmer[a,*], T.A. Palmer[a], S.S. Babu[b], E.D. Specht[b]

[a] *Lawrence Livermore National Laboratory, P.O. Box 808, L-355, Livermore, CA 94551, USA*
[b] *Oak Ridge National Laboratory, Oak Ridge, TN 37831, USA*

Received 7 June 2004; received in revised form 17 August 2004; accepted 27 August 2004

Abstract

In situ X-ray diffraction experiments using synchrotron radiation were performed on Ti–6Al–4V samples to directly observe the α → β phase transformation during heating. These experiments were conducted at the Advanced Photon Source (APS) using a 30 keV synchrotron X-ray beam to monitor changes in the α and β phases as a function of heating time under different heating rates. The results were compared to computational thermodynamic predictions of the phase fractions versus temperature, providing information about the kinetics of the α → β transformation in Ti–6Al–4V. The measured transformation rates were shown to be consistent with a diffusion-controlled growth mechanism, whereby diffusion of V in the β-Ti phase controls the rate. Based on the X-ray diffraction data, real time measurements of the α and β phase lattice parameters were made. Dramatic differences were observed in the changes of the lattice parameters of the two phases during the transformation. These changes are believed to be due to the partitioning of V and its strong effect on the lattice parameter of the β phase. An unexpected contraction of the lattice parameter of the β phase was further observed during heating in the temperature range between 500 and 600 °C. The origin of this contraction is most likely related to the annealing of residual stresses created by the different thermal expansion behaviors of the two phases.
Published by Elsevier B.V.

Keywords: X-ray diffraction; Synchrotron radiation; Thermal expansion; Annealing; Phase transformation; Kinetics; Vanadium partitioning; Diffusion; Lattice parameter; Residual stress

1. Introduction

Ti–6Al–4V is a titanium alloy with a two phase microstructure that is thermomechanically processed to create a desired amount of the α and β phases with a fine grain size for optimum mechanical properties. Microstructural characteristics such as grain size, β content, and β distribution influence its mechanical properties, which are highly dependant on the thermo-mechanical processing conditions [1,2]. Thermal cycles typical of welding and heat treating will significantly alter this carefully-prepared microstructure. Prediction of the effects of these thermal cycles on the microstructure is important in order to tailor a desired microstructure. In addition, the effects of less well-controlled welding processes on the microstructural evolution can be better understood and mitigated.

In order to develop a better understanding of microstructural evolution during welding, in situ X-ray diffraction observations of the phase transformations in Ti–6Al–4V were recently performed [3,4]. These experiments were conducted on both moving welds, where quasi-steady state heat flow conditions produced relatively low heating rates, and on spot welds where the heating and cooling rates were rapid. In the moving weld experiments [3], the effect of welding parameters on the α → β transformation were investigated, showing the kinetics of this transformation at low heating rates and the extent of the β phase field that forms in the heat affected zone of the weld. In the spot weld experiments [4], the α → β transformation kinetics were investigated and modeled by a Johnson–Mehl–Avrami approach, to produce a set of kinetic parameters for the prediction of the α → β phase transforma-

* Corresponding author. Tel.: +1 925 422 6543; fax: +1 925 423 7040.
E-mail address: elmer1@llnl.gov (J.W. Elmer).

0921-5093/$ – see front matter. Published by Elsevier B.V.
doi:10.1016/j.msea.2004.08.084

tion at high heating rates. In addition, the $\alpha \rightarrow \beta$ transformation on cooling was investigated at different weld locations, showing the effects of the weld location on the formation of α and α' martensite on cooling.

In the previous experiments, the temperature cycle produced by the welding arc was not well-controlled, and temperatures were not directly measured. To extract useful kinetic information from these data, the temperatures experienced during the weld heating and cooling cycles were calculated using a coupled thermal-fluids numerical code. This code enabled the temperatures in the weld heat affected and fusion zones to be calculated, and was accurate enough to determine heating rates, cooling rates and approximate temperatures where phase transformations were observed to initiate. However, some of the finer details of the $\alpha \rightarrow \beta$ phase transformation were not able to be measured with confidence due to the uncontrolled weld thermal cycle and some uncertainties about the actual temperature of the weld. Because of these uncertainties, a new set of experiments was performed to more closely observe the $\alpha \rightarrow \beta$ phase transformation under more controlled conditions.

In the current experiments, synchrotron-based X-ray diffraction was again used to directly observe the phase transformations during heating in Ti–6Al–4V, but this time using a different experimental setup whereby the samples are heated and cooled at controlled rates. These experiments complement the previous in situ welding experiments, and take a closer look at the lattice parameters and expansion rates of the α and β phases during the phase transformation on heating. The results of these experiments provide details about the individual contributions of each phase to the kinetics of the $\alpha \rightarrow \beta$ transformation, and show how the lattice expansion of the β phase is strongly affected by the combination of thermal and chemical effects during the $\alpha \rightarrow \beta$ phase transformation. These results will aid in the development and verification of numerical weld models for the prediction of Ti–6Al–4V microstructures during both welding and heat treating applications.

In situ X-ray diffraction measurements of the phase transformations of Ti–6Al–4V under isothermal conditions have been performed by other investigators as well [5,6]. Their results, however, were limited by an extremely long acquisition time per diffraction pattern, which ranged from 6 to 17 min, and the ability to study only a single, slow heating rate (20 K/min). The phase transformation was almost fully completed by the time the first diffraction pattern was acquired [5]. Secondly, these experiments used X-rays of 8.0 and 8.9 keV. The X-ray absorption lengths for Ti–6Al–4V at these energies are 12 and 16 μm, respectively. In another case [6], the researchers sampled a thin oxygen-rich surface layer, rather than bulk behavior. Surface effects were exacerbated by the slow heating rates and data acquisition. This work addresses these problems through rapid heating rates (up to 30 K/s), rapid data acquisition (3 s per diffraction pattern), and higher energy with more penetrating X-rays (30 keV, 528 μm absorption length).

2. Experimental procedures

2.1. Materials

A Ti–6Al–4V ELI (extra low interstitials) alloy was obtained in 100 mm diameter bar stock that had been mill annealed at 705 °C for 2 h then air cooled to room temperature. Chemical analysis showed that the alloy contained 6.0Al, 4.2V, 0.11O, 0.17Fe, 0.0028H, 0.014C, 0.009N, <0.03Si, bal. Ti, by wt%. Fig. 1 shows the microstructure of the starting material that was polished and chemically etched using a modified Kroll's solution containing 5 mL HF, 10 mL HNO_3, 30 mL lactic acid for approximately 30 s. This microstructure contains approximately 12% β distributed intergranularly around the slightly elongated α grains. The α grains of the starting material have an aspect ratio of approximately 2:1, with an average grain size of 5.8 μm across their small dimension.

The phase equilibria in Ti–6Al–4V are illustrated in the pseudobinary phase diagram shown in Fig. 2. These calculations were performed using ThermoCalc® [7] with the Ti-data data base (distributed by UES Software), and considered the influence of Ti, V, Al, Fe and O on phase equilibria at the nominal alloy composition. The vertical dotted line in this figure indicates the composition of the alloy being investigated, and shows that the amount of β will increase during heating, completely transforming to β at a temperature of 956 °C. Above this temperature, β is stable up to the solidus temperature of 1693 °C, and complete melting occurs at the liquidus temperature of 1701 °C. This calculated β transus temperature is slightly lower than one (975 °C) based on experimental measurements for nominally the same alloy [2]. Even though Ti_3Al is predicted in the equilibrium thermodynamic calculations, this phase was not observed in the starting microstructure.

Microchemical compositions of the starting α and β phases were determined using microprobe analysis. The data

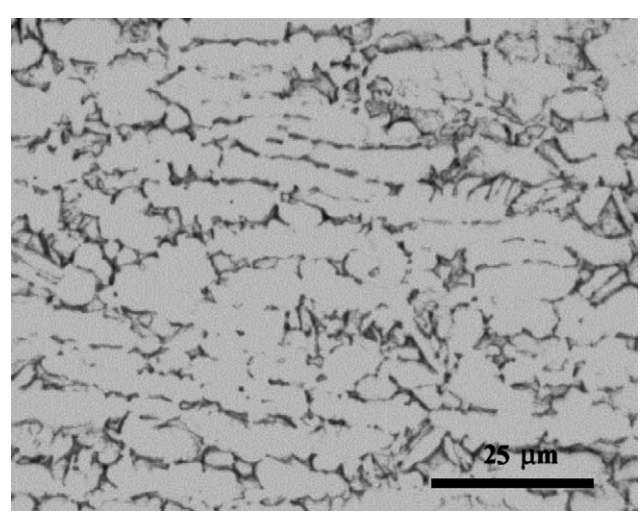

Fig. 1. Microstructure of the mill annealed Ti–6Al–4V base metal microstructure. The dark etching phase is β.

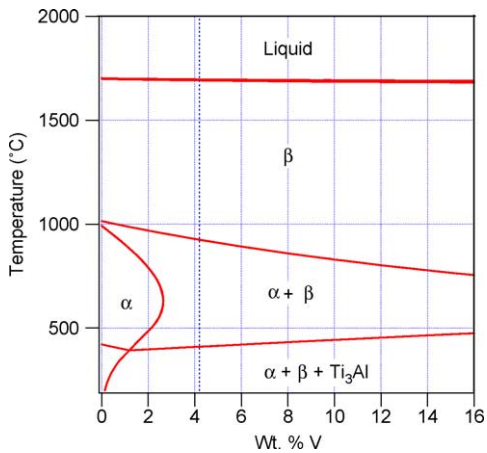

Fig. 2. Calculated pseudobinary phase equilibrium showing the influence of vanadium content on the α-Ti and β-Ti phase. The vertical dashed line represents the nominal alloy composition.

were collected on a JEOL-8200 microprobe, operating at 15 KV and a beam current of 20 nA. Individual point locations were inspected using a beam diameter of 1 μm, and a "broad beam" analysis was obtained by rastering 1 μm beam over 100 μm × 100 μm raster. X-ray intensities were calibrated using Ti, V, Al, Fe and SiO_2 for oxygen, and corrected to wt% using the ZAF corrections. The intensities were also run using TiO_2 and Al_2O_3 as standards and yielded result within error of those calibrated using Ti and Al. The results are shown in Table 1 and represent the average of seven measurements made at different locations for each phase. It is clear from these results that V and Fe partition to the β phase, while Al partitions to the α phase. In addition to the microchemical composition information, backscattered electron images taken of the polished surface were used to show the initial area fraction of β in the microstructure to be 12.1%.

Table 1
Chemical composition of the α and β phases in the base metal as measured by microprobe analysis

	Al	V	Fe	Ti
Nominal composition	6.2	4.0	0.17	92.5
β Phase	2.92 ± 0.11	15.43 ± 0.86	1.32 ± 0.11	80.7 ± 0.70
α Phase	6.73 ± 0.33	1.42 ± 0.73	0.04 ± 0.02	91.2 ± 0.47

Seven points were averaged into each composition and the one σ value is given as the estimated error. All values are in wt%.

2.2. In situ X-ray diffraction experiments

The X-ray diffraction measurements were performed on the UNICAT beam line BM-33-C at APS using a 30 keV X-ray beam from a ring current of 100 mA. This beam line was set up with a water-cooled Si(1 1 1) monochromator, and the beam was focused and sized to dimensions of 1 mm wide by 0.25 mm high using a dynamically bent Si crystal and collimator slits. The X-ray detector was manufactured by Roper Scientific (A99k401, RS/Photometrics). This CCD X-ray detector uses 2 in. × 2 in. array of 1024 pixels × 1024 pixels spaced 60 microns apart to capture the diffraction patterns produced on a scintillating screen connected to the CCD array using a fiber optic bundle. The experimental setup is shown in Fig. 3. Test coupons measuring 100 mm long by 4.75 mm wide by 2 mm thick were machined from the Ti–6Al–4V bar in an orientation parallel to the extrusion direction. All surfaces are milled to a 62 micron rms finish in preparation for the X-ray diffraction experiments. The coupons were clamped into a water-cooled copper fixture that allows high currents to be passed through them. Direct resistance heating of the coupon was used for rapid heating, while water-cooled grips allowed the sample to be rapidly cooled. The temperature of the sample was monitored and recorded using type-S

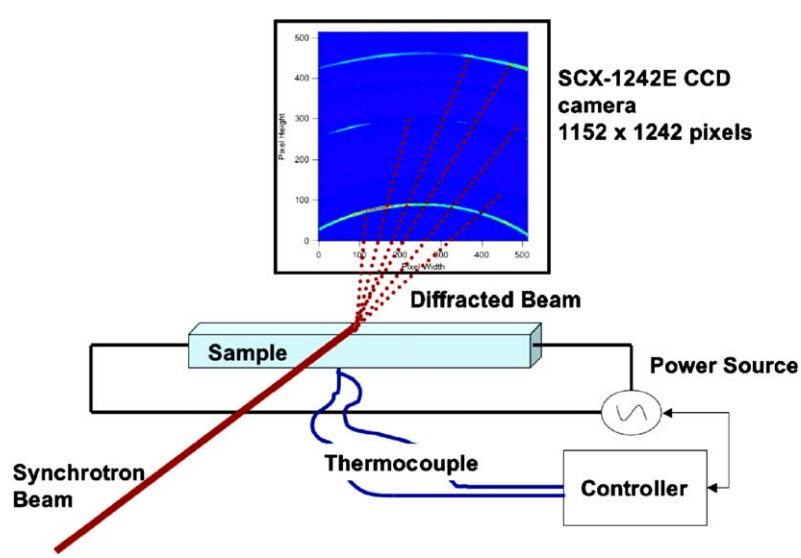

Fig. 3. Schematic of the X-ray setup used for in situ observations of phase transformations under controlled heating and cooling conditions.

(Pt/Pt–10%Rh) thermocouples, which are spot welded on the back side of the sample directly below the X-ray impingement point. A Eurotherm 818 temperature controller, a Eurotherm 425A power thyristor, and a Trindl RT300 transformer were used to control the AC current passing through the sample so that pre-programmed thermal cycles could be followed in a controlled manner. The entire assembly is covered with a canister in which high purity helium is introduced to minimize oxidation of the sample during high temperature runs. The heating power supply is capable of producing 300 A at 6 V and can heat the sample up to temperatures as high as 1400 °C. Heating and cooling rates on the order of 50 °C/s are possible.

While the sample is being heated, the X-ray beam impinges on the top surface of the sample at a 5° angle of incidence. The 528 μm X-ray absorption length provides a penetration depth of at least 23 μm, which can become larger at higher Bragg angles. The diffracted beams are collected using a CCD detector that is placed 330 mm behind the sample. The detector captures the X-ray data by integrating the diffracted beams over a 1 s exposure. Another 2 s are required to clear the data from the CCD detector and transfer it to the computer. Thus, it is possible to capture a complete diffraction pattern approximately every 3 s. The detector read-out is accelerated by a 2 × 2 binning of the pixels. An advantage of the 2D detector is that a larger number of grains satisfy the diffraction condition than do for a conventional $\theta/2\theta$ scan, so statistically valid diffraction data can be collected for more coarse-grained samples. One of the initial X-ray diffraction patterns of the Ti–6Al–4V base metal at room temperature is shown in Fig. 4a. In this figure, the Debye arcs of the diffracted beam are shown for a *d*-spacing range from 1.2 to 2.7 Å.

To calibrate the X-ray detector, the room-temperature lattice parameters of the base metal at room temperature were first measured using a conventional Cu Kα X-ray diffraction system. A room-temperature pattern is then collected using the CCD with synchrotron radiation. Five points are selected along each of 3 Debye arcs. Finally, the sample-detector distance, the position of the center of the arcs on the detector, and the magnitude and orientation of the detector tilt are varied to minimize the difference between the *d*-spacing at the selected points as calculated from these detector patterns and that calculated from the lattice parameters. Using this calibration, the Debye arcs are converted into a 1-D plot showing diffracted beam intensity versus *d*-spacing using Fit-2D software [8,9]. This software integrates the diffracted beam intensity for each arc over the entire 2-D areal array, creating the diffraction pattern shown in Fig. 4b. Since this alloy contains approximately 88% α-Ti at room temperature, the diffraction pattern is dominated by the hcp α-Ti diffraction peaks. In this diffraction pattern nine α-Ti peaks and two β-Ti peaks are present.

The amounts of α and β phases present at each time increment were then calculated using an analysis of the peaks present in each diffraction pattern [10]. The lattice spacing,

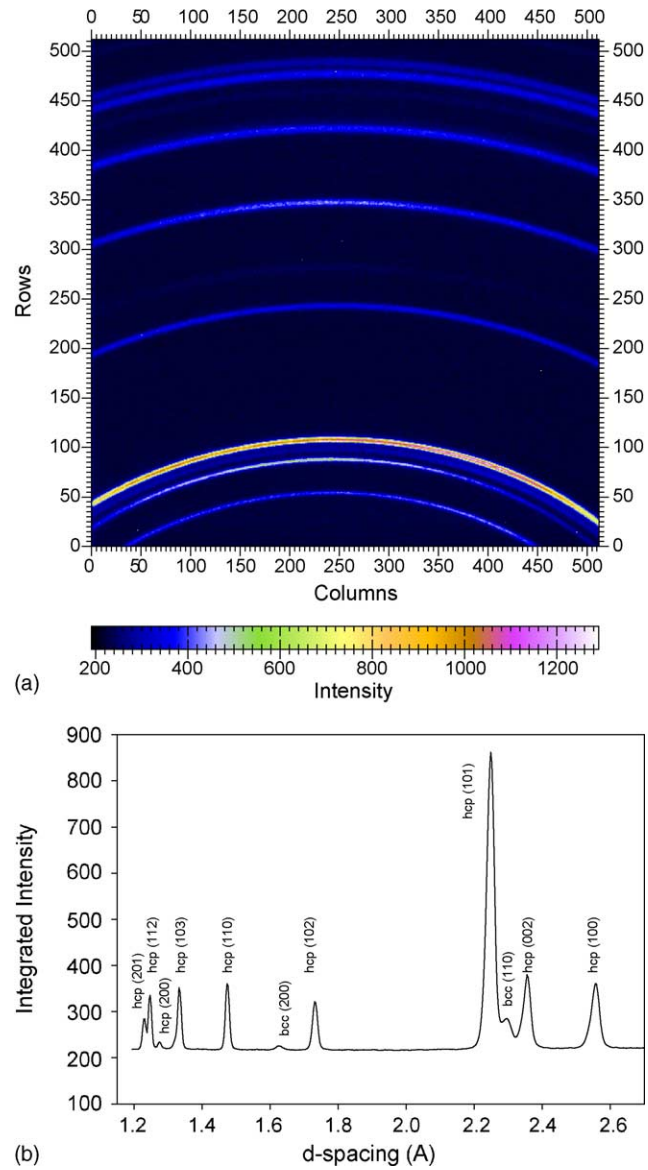

Fig. 4. Initial diffraction pattern of the Ti–6Al–4V sample at room temperature. (a) Debye arcs as imaged on the CCD areal X-ray detector and (b) shows this same data converted into an integrated intensity vs. *d*-spacing plot.

FWHM value, and integrated intensity of each peak were determined using an automated curve-fitting routine developed in Igor Pro®, Version 4.0. In this routine, a sum of one or more Gaussian peak profile fitting functions is applied to each peak and the values of these fitted peaks are then reported.

The amount of the β phase was determined by first taking the ratio of the area of the β phase peaks to the total diffraction peak area (β/(α + β)). Due to differences in the diffraction conditions of the two phases this area fraction does not equal the true β fraction of the alloy. However, since the starting amount of β in the microstructure is known through metallographic measurements (12.1 vol%), a correction could be made to convert the X-ray diffraction peak area measurements into volume fraction β. This normalization factor was

then applied to all of the X-ray diffraction patterns obtained during heating cycle to determine the amount of β as a function of temperature. The fraction of α was then determined for each measurement by subtracting the measured β fraction from unity, since only these two phases are present in the microstructure.

3. Results and discussion

3.1. The α → β phase transformation during heating

Since equilibrium is rarely attained during welding or heat treating of alloys, the microstructures that form can be considerably different than those expected from the equilibrium phase diagram, such as the one shown in Fig. 2 for Ti–6Al–4V. Therefore, it is generally not possible to predict microstructural evolution from the phase diagram without knowing additional information about the kinetics of the phase transformations taking place. Thermal cycling adds another level of complexity in predicting microstructural evolution, since the microstructures that form during heating are subsequently altered by the transformations that take place during cooling. It is thus useful to be able to follow the sequence of events that lead up to the final microstructure using in situ experiments.

To better understand the evolution of microstructures during heating, in situ X-ray diffraction techniques were used to directly observe changes in the crystal structure of this Ti–6Al–4V alloy and to measure the relative amounts of the α and β phases under controlled heating conditions. Fig. 5 shows the results from nine different samples heated at rates of approximately 30 °C/s to peak temperatures between 600 and 1000 °C. The amount of β phase increased with increasing peak temperature and each sample followed the same trend during the initial stages of heating. This trend is compared to the thermodynamic predictions, which are represented by the dashed line on the plot. These predictions show the equilibrium condition for this alloy.

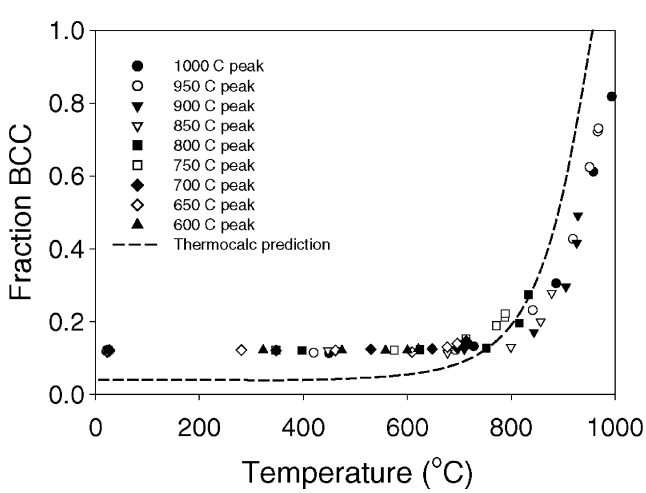

Fig. 5. TRXRD measured bcc phase fraction in the HAZ of the Ti–6Al–4V during continuous heating (symbols), and thermodynamic prediction (dashed line).

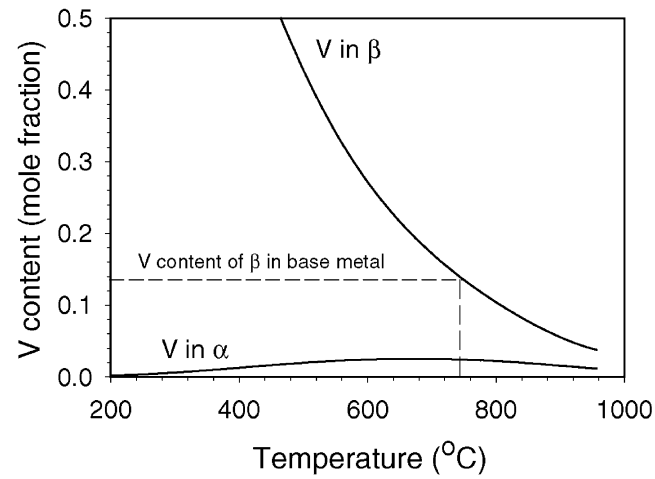

Fig. 6. Calculated vanadium content of the α and β phases as a function of temperature, showing the strong partitioning of vanadium to β as the temperature decreases. The dashed lines indicate the measured vanadium content of the β phase in the starting microstructure, and its corresponding equilibrium temperature.

Significant differences exist between the measured and calculated amounts of β as a function of temperature. First, the β content of the starting base metal is 12.1% instead of about 4% predicted from equilibrium thermodynamics. This difference occurs during manufacturing of the Ti–6Al–4V bar, which was mill annealed at 705 °C then rapidly cooled to room temperature. Since the α → β phase transformation is controlled by diffusion, only a small fraction of the β formed at high temperatures will transform to α during the rapid air cooling of the initial Ti–6Al–4V ingot [11], resulting in a higher initial volume fraction β at room temperature than predicted by thermodynamics.

In addition to the different amount of β phase at room temperature, its composition will be different than that predicted by thermodynamics. For example, a lower V content than that predicted by equilibrium thermodynamics will be present in the β phase of the sample, since the V would not be able to completely diffuse during the initial cooling of the ingot. The calculated amount of V in the β phase is shown as the solid line in Fig. 6. This prediction is compared to the measured value of V in β at room temperature (dashed line). At low temperatures, the calculated V content of the β phase should be in excess of 50% [4]. However, the V content measured in the base metal is only 15.4 ± 0.86 wt% (13.6 ± 0.76 mol%), which would correspond to an equilibrium V concentration in this alloy at a temperature of approximately 750 °C. This temperature closely corresponds with the original mill annealing temperature of this alloy, suggesting that very little diffusion occurred during cooling. Furthermore, this temperature should correspond to the temperature where the α → β transformation should occur during heating. The exact temperature will depend on the heating rate.

Another observation regarding the data presented in Fig. 5 is that complete transformation to β was not observed at the β transus temperature. The possible reason for this is related to two effects. One factor is that oxygen can react with titanium and titanium alloys at elevated temperatures and stabilize the α phase [2]. Although the experiments were performed using an inert gas purge, some discoloration of the samples was observed after removing them from the experimental apparatus. Although no obvious oxide phases were observed in the diffraction patterns, diffusion of oxygen into the titanium likely occurred to some degree and could have contributed to the presence of α at temperatures above the calculated β transus [12]. The observed α fraction at 1000 °C corresponds to 0.4 wt% O [6]. A second factor is that the effect of temperature on the intensity of the diffracted beams was not taken into account [13]. This effect may result in an underestimation of the measured amount of β phase at high temperatures [5], due to the fact that β displays a larger lattice expansion than α, as will be discussed in more detail later.

Metallographic sections were prepared from three of the samples, heated to peak temperatures of 800, 900 and 1000 °C. These microstructures are compared in Fig. 7a–c, showing the effects of increasing amounts of transformation on the microstructure as the peak temperature increases. Fig. 7a shows the microstructure of the sample heated to a peak temperature of 800 °C, where only a small fraction of the α phase had transformed to β. The dark etching regions of the microstructure correspond to regions where the β phase was the most concentrated. These regions appear diffuse in comparison to the base metal microstructure, indicating that some transformation and diffusion has taken place. Fig. 7b shows the microstructure of the sample heated to a peak temperature of 900 °C, where approximately 15% of the α phase had transformed to β. In this micrograph, the dark etching β phase regions of the base metal appear to be gone, indicating increased transformation and diffusion at this temperature. The lightest etching regions in this micrograph correspond to the α phase that was untransformed at the peak temperature. Fig. 7c shows the microstructure of the sample heated to a peak temperature of 1000 °C, where complete, or near complete, transformation to the β phase occurred prior to cooling. This microstructure is significantly different that the others and consists mostly of acicular α. The acicular α phase was created during cooling from the large grained β structure formed during heating and is characteristic of the microstructures that form during rapid cooling from the β phase field.

Fig. 5 also showed a significant difference between the measured and calculated amounts of the β phase at each temperature, indicating that the α → β transformation requires higher temperatures, approximately 50 °C, than those predicted by equilibrium thermodynamics for temperatures above 800 °C. This amount of superheating is required to reach a given amount of β phase in the microstructure, and is related to the kinetics of the α → β transformation, which requires a finite amount of time to occur.

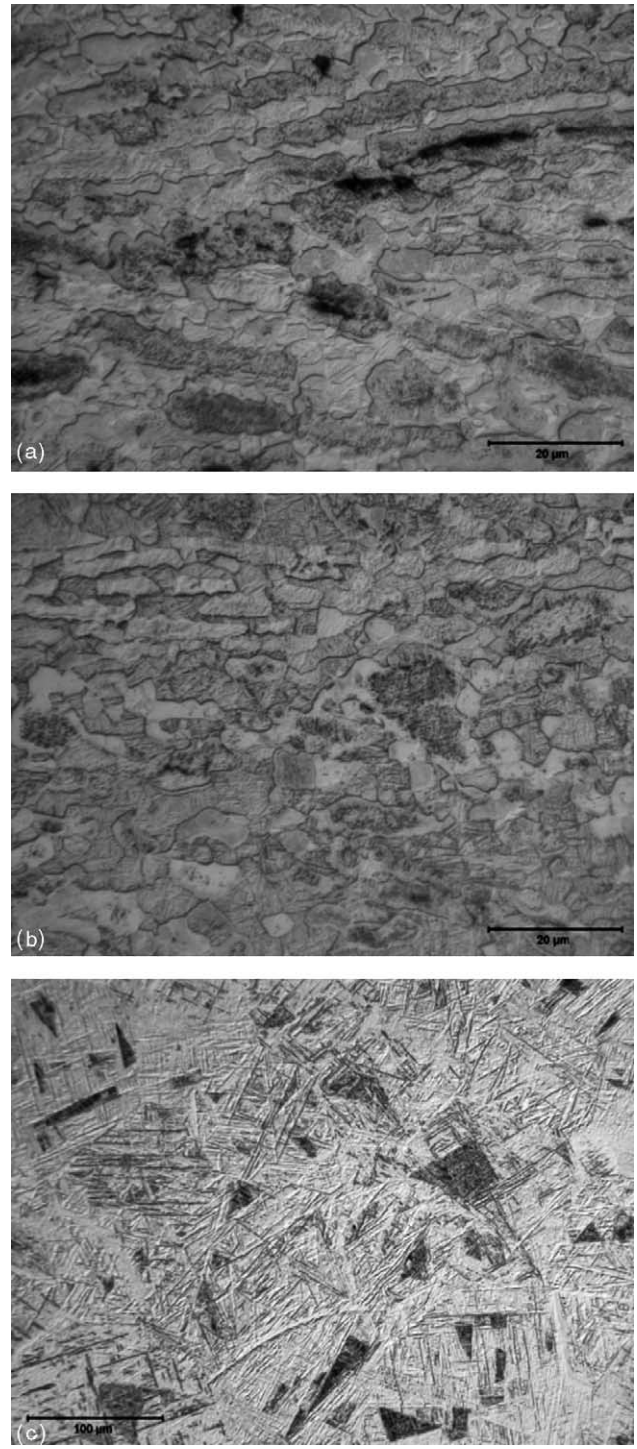

Fig. 7. Micrographs of the Ti–6Al–4V samples after heating to peak temperatures of (a) 800 °C, (b) 900 °C and (c) 1000 °C. Note the decreased magnification in (c).

It is clear from the above results that non-equilibrium conditions are affecting the α → β transformation. Additional experiments were performed to determine the effects of heating rate on the transformation rate. In these experiments, two samples were heated at an initial rate of 10 °C/s to 500 °C. The heating rate on the first sample was then decreased to

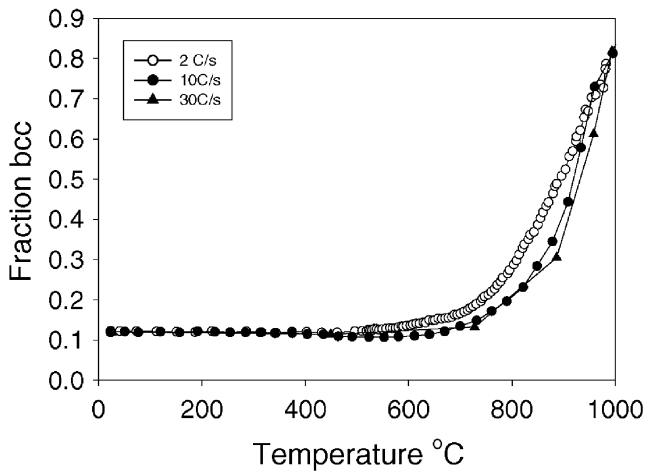

Fig. 8. Measured β phase fraction plotted vs. temperature during heating for three different heating rates.

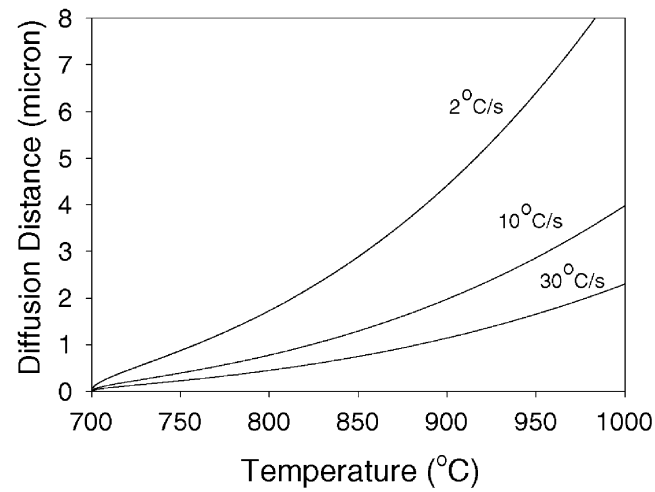

Fig. 9. Calculated diffusion distance of V in the β phase at three different heating rates.

2 °C/s, while the other sample continued heating at 10 °C/s to 1000 °C. The experimentally measured amounts of β as a function of temperature from these samples were then compared to the data taken at a constant heating rate of 30 °C/s.

Fig. 8 compares the amount of β measured in each of the three heating rate experiments as a function of temperature. Deviations from the calculated equilibrium values are observed as the heating rate is increased. These deviations are such that the samples heated at the lower rates show a higher β fraction than the samples heated at the higher rates. At a temperature of approximately 925 °C, the measured fractions of transformed β become equal for the samples heated at rates of 2–10 °C/s. Based on these results, it appears that the transformation kinetics are limiting the transformation rate for the sample heated at a rate of 10 °C/s at temperatures below 925 °C. At this temperature, diffusion appears rapid enough to compensate for the higher heating rate. Even larger deviations are observed in the sample heated at a rate of 30 °C/s, where a temperature of 1000 °C is required for diffusion to catch up with the high heating rate.

Diffusion calculations were then performed to estimate the diffusion distance and amount of transformation expected at the different heating rates. In these calculations, the diffusion of V in the β phase is used to represent the growth controlled $\alpha \rightarrow \beta$ phase transformation that occurs during heating [11]. The diffusion coefficient for V in β has been measured and can be represented by an Arhennius expression [$D = A\exp(-Q/RT)$] with an activation energy (Q) of 123.9 kJ/mole and a pre-exponential (A) of 1.6×10^{-4} cm^2/s for a binary Ti–V alloy containing 10 at.% V [14]. Using this relationship to represent the diffusion coefficient as a function of temperature (T), the diffusion distance was calculated from the relationship $X(t) = 2(Dt)^{1/2}$, where X is the diffusion distance and t is the time [15]. The time is related to the constant heating rate by the differential expression $\mathrm{d}t = R\,\mathrm{d}T$, where R is the imposed heating rate.

The diffusion distance was then estimated by integrating $X(t)$ over the heating cycle of the weld, starting at the mill anneal temperature of 705 °C. Fig. 9 plots the results, showing how far V will diffuse as a function of temperature at the three different heating rates. For each condition, the calculated diffusion distance increases at an increasing rate as the temperature increases. These calculations show that the diffusion distance at 1000 °C is about 9 μm at 2 °C/s, 4 μm at 10 °C/s and 2.3 μm at 30 °C/s. Comparing these data to the scale of the microstructure gives an indication of how much transformation can be expected to occur. The average grain size of the base metal was measured to be 5.8 μm across the small dimension of the grains, and since only one-half of this distance (2.9 μm) is required to transform the microstructure, it would be expected that the two slower heating rates are capable of completely transforming the microstructure during their heating cycle. At the highest heating rate of 30 °C/s, the diffusion distance is slightly smaller than the microstructural scale, indicating that a small amount of untransformed β phase may exist when the sample first reached 1000 °C. Additional experiments are planned to investigate the effects of heating rate on the transformation kinetics of Ti–6Al–4V.

3.2. Lattice expansion of the α and β phases

The lattice parameter of the α and β phases were determined from the 2θ positions of their respective diffraction peaks. The lattice parameter, a_0, for the β phase was determined from the bcc (1 1 0) peaks, and the lattice parameter, a, for the α phase was determined from the hcp (1 0 1) peaks, assuming the c/a ratio is equal to 1.5963, which corresponds to the value in the base metal at room temperature. These two peaks represent the strongest diffraction peaks for each phase, and provided good measurements of the lattice parameter throughout the entire heating range. In Fig. 10, the lattice parameters are plotted as a function of temperature for heating rates of 2 and10 °C/s.

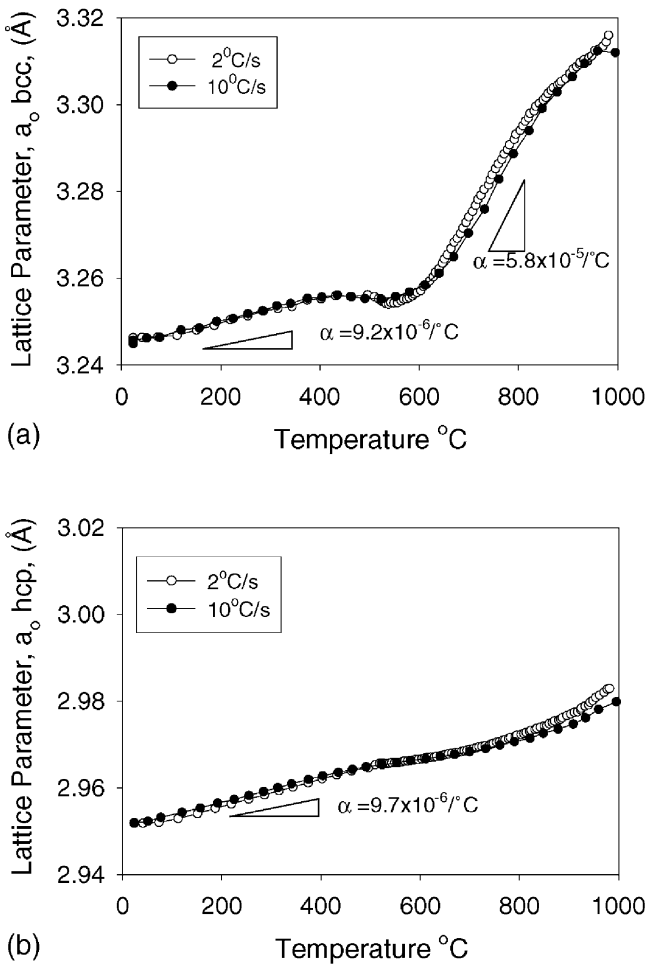

Fig. 10. Measured lattice parameters as a function of temperature for both the (a) bcc and (b) hcp phases as a function of temperature during heating at two different rates. The indicated coefficients of thermal expansion, α, were calculated from the slopes of the curves.

Before the α → β transformation begins, the crystal lattice expands as a result of the thermal expansion effects during heating. The thermal expansion coefficient for Ti–6Al–4V is reported to be between 8.5×10^{-6} and 10×10^{-6}/°C near room temperature [2,5]. These values correspond very well with the experimentally measured thermal expansion coefficients for the α (9.7×10^{-6}/°C) and β (9.2×10^{-6}/°C) phases shown in Fig. 10. Considering the alloy consists mostly of α near room temperature, the weighted average lattice expansion of the two phase mixture should be closer to that of the α phase. As the α → β transformation takes place, the ratio of β to α increases and the expansion of the β phase should dominate.

The results presented in Fig. 10 display a dip in the lattice parameter of the β phase near the beginning of the α → β transformation. This dip is followed by a rapid increase in the rate of change to a value of 5.8×10^{-5}/°C, which is approximately 6× that observed at lower temperatures. During these significant changes in the β phase lattice expansion, the α phase undergoes only a slight decrease in the lattice expansion rate, reaching a minimum at 750 °C before increasing again at higher temperatures. The different behaviors of the two phases during the α → β transformation are most likely explained by the diffusion of alloying elements, and can be understood by comparing the variations in composition of each phase as a function of temperature.

Thermodynamic calculations of the Al and V content of each phase show that the Al content of each phase changes little with temperature. However, the V content, particularly of the β phase, changes significantly [4]. As shown in Fig. 6, the β phase shows a dramatic variation in V content, from about 0.95 to 0.04 mol fraction, from room temperature to the β transus temperature under equilibrium conditions [4]. In addition, it is known that by increasing the V content, the lattice parameter of the β phase will decrease. For example, the lattice parameter of β decreases from 3.26 to 3.21 as the V content increases from 11 to 19 wt% [16]. Therefore, as the α → β transformation takes place, the V is spread out over an increasingly larger volume fraction of the β phase, which reduces the concentration of V in β. This decrease in V content increases the lattice parameter for the β phase beyond that caused by thermal effects alone.

While the β phase is undergoing this rapid expansion, there is a much smaller, but clearly measurable, decrease in the expansion rate of the α phase between 550 and 750 °C. This behavior can also be explained by the partitioning of V. Since the V content of the α phase goes through a maximum at about 700 °C, as indicated in Fig. 6, then the X-ray diffraction results suggest that increasing the V content of the α phase would decrease its lattice parameter. Published data regarding the influence of V on the lattice parameters of α titanium confirm a decrease in both the *a* and *c* lattice parameters with increasing V content [17]. Thus, the behaviors of the lattice parameters of both the α and β phases can also be explained by the partitioning of V to the respective phases, in addition to the thermal effects, as the α → β transformation proceeds.

The effect of heating rate on the lattice parameters of the α and β phases is also shown in Fig. 10. With increased heating rate, the changes in lattice parameter are delayed to higher temperatures, but otherwise show similar behaviors. This correlation is also consistent with the effects of heating rate on the β phase fraction with temperature. Since higher temperatures are required to transform a given amount of β at the higher heating rates, the changes in lattice parameter are shifted to higher temperatures as well. At the higher heating rate, the dip in the lattice parameter of the phase that occurs at about 550 °C is less pronounced, indicating that this dip has a rate dependence.

The origin of this dip is not known but is most likely related to one of three possible effects. One possibility is the diffusion of V to the β phase at low temperatures in order to compensate for the non-equilibrium starting condition of the base metal. A second possibility is the relaxation of residual stresses that are built up in the two phase mixture of the alloy when it is cooled to room temperature during processing. A third possibility is the formation of ω phase from the β phase that can occur

at these temperatures [2,17]. However, no evidence of the ω phase was observed in the X-ray diffraction experiments. The other two possible effects will be looked at separately.

First, there clearly is a driving force for the transformation of the non-equilibrium β phase to α during heating at temperatures less than the mill annealing temperature of the alloy. This driving force is the difference between the amount of β in the base metal (12.1%) and that predicted by thermodynamics (4%). Thus, with a decrease in the amount of β phase, there would be a corresponding increase in its V content and decrease in its lattice parameter. However, diffusion of V to a measurable extent at these heating rates would be difficult, due to the low diffusivities of V in titanium at these relatively low temperatures [2,11]. Furthermore based on the synchrotron results, there appears to be no significant amount of α → β transformation occurring at these temperatures, since the initiation of the dip appears to precede the observed initiation of the transformation.

The other possible mechanism for the dip is the relaxation of residual stresses. Differences in the coefficients of thermal expansion of the α and β phases will create internal stresses in the multiphase mixture as the alloy cools from its mill annealing temperature. In addition, transformation strains may be present due to the differences in densities of the α and β phases [18,19]. It may be possible that these stresses begin to anneal out in the 500–600 °C temperature range, just before the α → β phase transformation begins to occur, thus creating the dip. Additional work is planned to study this effect in future synchrotron experiments.

The overall expansion of the multi-phase mixture can be estimated from the lattice expansions of the two individual phases and their relative fractions in the microstructure. This calculation can be made by first determining the volume of the hcp unit cell of the α phase ($a^2c\sin(60°)$), and the volume of the bcc unit cell of the β phase ($a_0{}^3$) as a function of temperature. These data are plotted in Fig. 11a for the α and β phases at the two heating rates. It is clear that the difference in unit cell volumes between the two phases decreases with increasing temperature since the β phase expands more than the α phase with increasing temperature. Near the end of the transformation, the unit cell volumes for the α and β phases become nearly the same. The heating rate, in the 2–10 °C/s range, seems to have little effect on the unit cell volumes of the two phases as a function of temperature.

The results from Fig. 11a were then used to estimate the overall expansion coefficient of the α + β two phase alloy by multiplying each unit cell volume by its respective volume fraction in the microstructure at each temperature. The sum of these two volumes represents the average volume of the α + β multi-phase mixture as a function of temperature. From this data, the average linear expansion coefficient of the alloy was estimated by taking the cube root of the volume expansion data. These results are shown in Fig. 11b for the two heating rates. In this plot, the average lattice expansion begins at a rate of 9.5×10^{-6} °C/s, and continues at this rate up to a temperature of approximately 500 °C. At

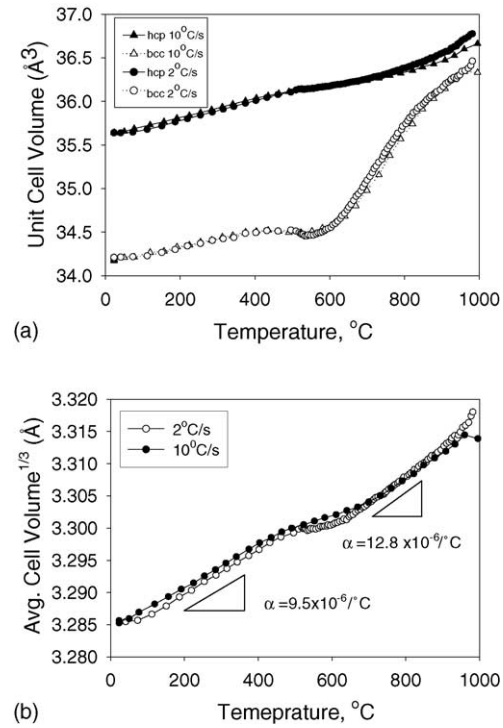

Fig. 11. (a) Measured unit cell volume for each phase at the two different heating rates plotted vs. temperature. (b) Cube root of the unit cell volumes plotted vs. temperature representing the average linear expansion for the multi-phase Ti–6Al–4V alloy. The indicated linear expansion coefficients, α, were calculated from the slopes of the curves, before and during the transformation.

this point, the expansion rate decreases, due to the dip in the lattice parameter of the β phase. Once the α → β transformation begins, the lattice expansion rate increases to an average value of 12.8×10^{-6} °C/s, and continues with this expansion rate throughout the α → β transformation temperature range. The heating rate appears to have only a slight influence on the average lattice expansion behavior, particularly in the 500–600 °C range, where the higher heating rate provides a smoother transition between the low temperature and high temperature expansion rates.

4. Conclusions

(1) In situ X-ray diffraction experiments performed on Ti–6Al–4V samples heated to different peak temperatures were used to directly observe the α → β phase transformation. At a heating rate of 30 °C/s, higher temperatures, on the order of 50 °C, were required to produce the same amount of β phase as that predicted by equilibrium thermodynamics.

(2) Controlled heating rate experiments were performed on samples heated to the β transus temperature at two different rates. The measured fraction of β indicated that the sample heated at 2 °C/s begins to show an increase in β at lower temperatures than the sample heated at 10 °C/s.

Transformation kinetics were shown to limit the transformation rate of the sample heated at 10 and 30 °C/s up to temperatures of 925 and 1000 °C, respectively. Above these temperatures, diffusion appeared rapid enough to compensate for the higher heating rate.

(3) Lattice parameter measurements of the α and β phases during heating showed the individual contributions of each phase to the overall lattice expansion of the alloy. Before beginning the $\alpha \rightarrow \beta$ transformation, the expansion coefficient of the α phase was slightly larger than that for the β phase. However, during the $\alpha \rightarrow \beta$ phase transformation, the expansion coefficient of the β phase increased dramatically to approximately 6× its low temperature value, while that of the α phase decreased slightly before passing through a minimum value.

(4) During the transformation, calculations of the average concentration of V in the β phase show a decrease from about 15–4%, while that of the α phase was calculated to go through a maximum of 2.5% at 750 °C. The change in V content of each phase and its effect on the lattice parameters can explain the different expansion behaviors of the two phases during the $\alpha \rightarrow \beta$ transformation.

(5) A dip in the lattice parameter of the β phase was observed just prior to the $\alpha \rightarrow \beta$ transformation. The origin of this dip is not known, but is most likely related to the relaxation of internal residual stresses that were created by the different lattice expansion/contraction rates of the α and β phases.

(6) The average thermal expansion coefficient of the two phase α + β mixture was calculated from the expansion of the two phases and the measured fractions of each as a function of temperature. There was an increase from 9.5×10^{-6}/°C at low temperatures to 12.8×10^{-6}/°C during the $\alpha \rightarrow \beta$ phase transformation. A decreased expansion is observed at temperatures between 500 and 600 °C, coinciding with a dip in the β phase lattice parameter. Expansion in the 500–600 °C temperature range shows a slight heating rate dependence whereby the change in expansion is lessened at higher heating rates.

Acknowledgments

This work was performed under the auspices of the U.S. Department of Energy, Lawrence Livermore National Laboratory, under Contract No. W-7405-ENG-48, and the LLNL portions of this work were supported by DOE, Office of Basic Energy Sciences, Division of Materials Science. Part of the research was sponsored by the U.S. Department of Energy Division of Materials Sciences and Engineering under contract No. DE-AC05-00OR22725 with UT-Battelle, LLC. The UNICAT facility at the Advanced Photon Source (APS) is supported by the U.S. DOE under Award No. DEFG02-91ER45439, through the Frederick Seitz Materials Research Laboratory at the University of Illinois at Urbana-Champaign, the Oak Ridge National Laboratory (U.S. DOE contract DE-AC05-00OR22725 with UT-Battelle LLC), the National Institute of Standards and Technology (U.S. Department of Commerce) and UOP LLC. The APS is supported by the U.S. DOE, Basic Energy Sciences, Office of Science under contract No. W-31-109-ENG-38. The authors express gratitude to Mr. Bob Vallier of LLNL for performing optical metallography.

References

[1] M. Donachie Jr., Titanium A Technical Guide, ASM International, 1989.
[2] Material Properties Handbook: Titanium Alloys, ASM International, 1994.
[3] J.W. Elmer, T.A. Palmer, J. Wong, J. Appl. Phys. 93 (2003) 1941–1947.
[4] J.W. Elmer, T.A. Palmer, S.S. Babu, W. Zhang, T. Debroy, J. Appl. Phys. 95 (2004).
[5] R. Pederson, O. Babushkin, F. Skystedt, R. Warren, Mater. Sci. Technol. 19 (2003) 1533–1538.
[6] S. Malinov, W. Sha, Z. Guo, C.C. Tang, A.E. Long, Mater. Charact. 48 (2002) 279–295.
[7] B. Sundman, B. Jansson, J. Andersson, Calphad-Comput. Coupling Phase Diagrams Thermochem. 9 (1985) 153.
[8] A.P. Hammersley, FIT2D V9.129 Reference Manual V3.1, ESRF Internal Report, ESRF98HA01T, 1998.
[9] A.P. Hammersley, S.O. Svensson, M. Hanfland, A.N. Fitch, D. Häusermann, High Press. Res. 14 (1998) 235–248.
[10] T.A. Palmer, J.W. Elmer, J. Wong, Sci. Technol. Weld. Joining 7 (2002) 159–171.
[11] S. Malinov, Z. Guo, W. Sha, A. Wilson, Metall. Mater. Trans. A 32A (2002) 879–887.
[12] T. Ressler, J. Wong, J.W. Elmer, J. Phys. Chem. B 102 (1998) 10724.
[13] J.W. Elmer, T.A. Palmer, W. Zhang, B. Wood, T. DebRoy, Acta Mater. 51 (2003) 3333–3349.
[14] C.J. Smithells, E.A. Brandes, G.B. Brook, Smithells Metal Reference Book, seventh ed., Butterworth-Heinemann Ltd., Oxford, UK, 1992.
[15] P.G. Shewmon, Diffusion in Solids, McGraw-Hill, New York, 1963.
[16] R. Castro, L. Séraphin, Mémoires Scientifiques Revu de Métallurgie 63 (1966) 1024.
[17] L.-c. Ming, M.H. Manghnani, K.W. Katahara, Acta Metall. 29 (1981) 479–485.
[18] C. Schuh, D. Dunand, Acta Mater. 49 (2001) 199–210.
[19] W. Szkliniarz, G. Smolka, J. Mater. Process. Technol. 53 (1995) 413–422.